A Gas-Capture Buoy for Measuring Bubbling Gas Flux in Oceans and Lakes

LIBE WASHBURN

Institute for Computational Earth System Science, Department of Geography, University of California, Santa Barbara, Santa Barbara, California

CYRIL JOHNSON

Physics Electronics Shop, University of California, Santa Barbara, Santa Barbara, California

CHRIS C. GOTSCHALK

Marine Science Institute, University of California, Santa Barbara, Santa Barbara, California

E. THOR EGLAND

Department of Geological Science, University of California, Santa Barbara, Santa Barbara, California

(Manuscript received 22 June 2000, in final form 8 January 2001)

ABSTRACT

The design, calibration, and deployment of a buoy and gas-capture assembly for measuring bubbling gas flux in oceans and lakes are described. The assembly collects gas in a chamber while continuously measuring the position of the gas–water interface that forms as gas accumulates. Interface position is determined from the differential pressure between the chamber and ambient seawater. A spar buoy provides flotation and stability to reduce vertical motion from surface waves. The gas-collection assembly and spar, referred to as a flux buoy, is suitable for deployment from small boats under conditions of light wind and small waves. The flux buoy is being used to determine the spatial distribution of natural hydrocarbon seepage off the south-central California coast. Hydrocarbon seepage from continental shelves may be an important source of atmospheric methane.

1. Introduction

In some water bodies, bubbles originating at the sea floor contribute significantly to the total flux of methane and other gases to the local atmosphere. For example, methane generated by thermogenic and bacterial processes beneath the seafloor can form plumes of rising bubbles extending to the sea surface (Hovland et al. 1993). This occurs strongly offshore of Coal Oil Point near Santa Barbara, California, where natural hydrocarbon seepage produces extensive, dense bubble plumes (Fischer 1977; Hornafius et al. 1999; Quigley 1997; Quigley et al. 1999). Natural hydrocarbon seeps occur elsewhere on continental shelves, including the Gulf of Mexico (MacDonald 1998), the Gulf of California (Simoneit et al. 1990), and the North Sea (Hovland et al. 1993). Gaseous marine hydrocarbon seepage is potentially an important source of atmospheric methane (Hovland et al. 1993).

Corresponding author address: Libe Washburn, Institute for Computational Earth System Science, Department of Geography, University of California, Santa Barbara, Santa Barbara, CA 93106-3060. E-mail: washburn@icess.ucsb.edu

Bubbling gas from sediments also contributes to the atmospheric flux of methane and other gases from lakes. Crill et al. (1988) found that methane flux from bubbles in an Amazonian floodplain lake was much greater than the diffusive flux and made up most of the total flux. In Mono Lake, California, natural gas seeps produce strong, localized methane flux, accounting for about 7% of the total flux over the lake surface (Oremland et al. 1987; Romero 1996). Chanton et al. (1988) describe large variations in bubbling methane flux on tidal and seasonal timescales from sediments in a freshwater tidal estuary in eastern North Carolina. An extreme example of bubbling gas flux occurred in Lake Nyos, Camaroon, during a deadly outgassing of carbon dioxide (CO_2) in August 1986 (Freeth and Kay 1987; Kanari 1989). Woods and Phillips (1999) use numerical simulations to examine how turbulent bubble plumes might produce large CO_2 fluxes to trigger gas eruptions in lakes.

Quantifying the bubbling flux of methane and other gases to the atmosphere from oceans and lakes is important for estimating global budgets. However, some sources, such as natural marine seepage, are poorly constrained because of a lack of measurements. To estimate

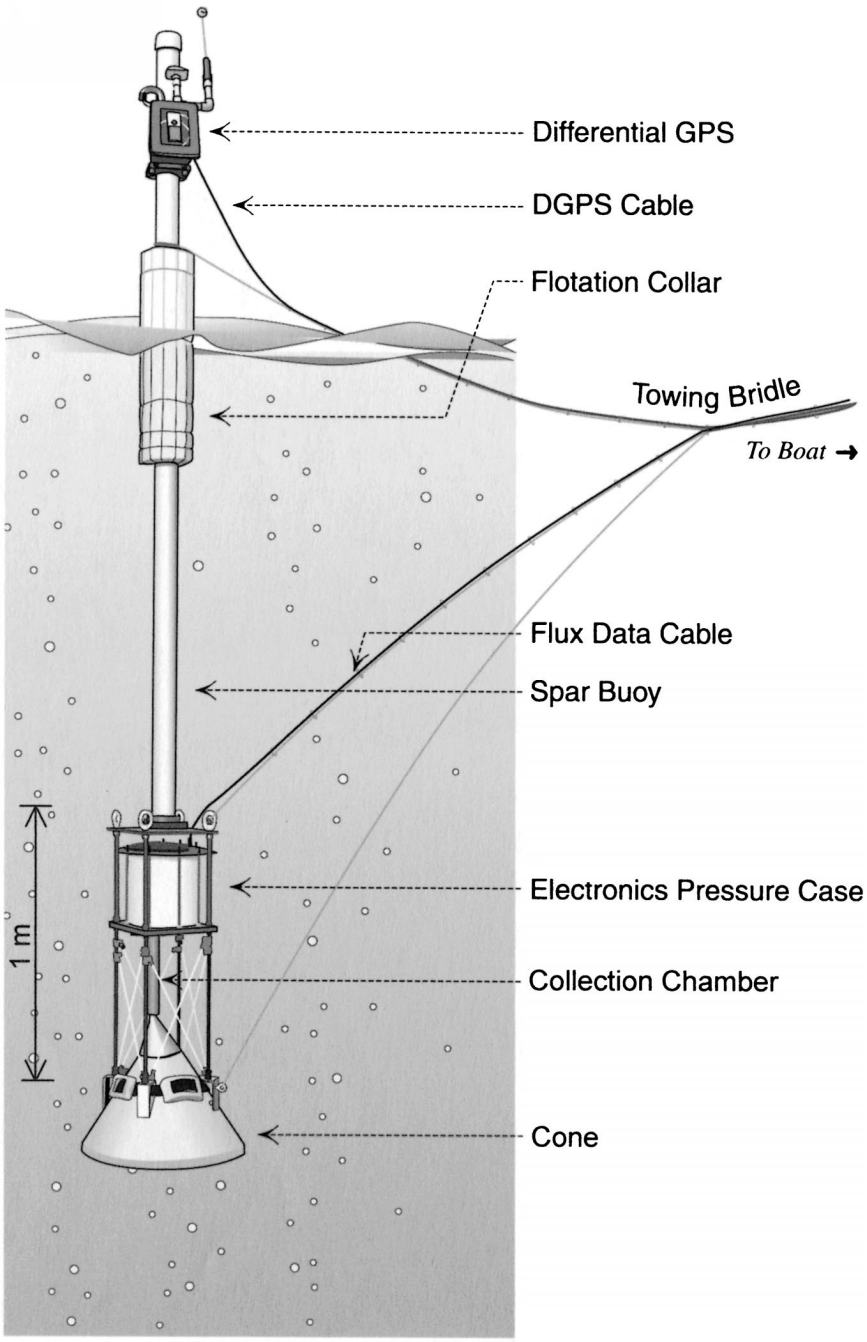

FIG. 1. Schematic of flux buoy. Electronics pressure case contains sensors, electronics, gas release valve, and microcomputer. Diagonal white lines around collection chamber are tensioned cables to provide stiffness. Scale at left indicates 1 m. (Bubble size is exaggerated.)

the hydrocarbon seepage contribution to the global methane budget, it is assumed that the spatial distribution of seeps is lognormal, but this has not been verified by observation (Hovland et al. 1993). Few systems for direct measurement of bubbling gas flux have been reported. One example, developed by Sebacher and Harriss (1982), used a floating gas collection chamber and detector system for measuring the diffusive and bubbling flux of methane in lakes and protected waters. This instrument was used in the study by Crill et al. (1988). Oremland et al. (1987) measured methane flux from natural gas seeps in Mono Lake by timing the capture of gas in a collection bottle. Chanton et al. (1988) deployed a floating pyramidal sampler to collect methane bubbles rising from sediments in an estuary. Flux was measured by allowing gas to accumulate over timescales

TABLE 1. Pressure and temperature sensor characteristics.

Sensor	Manufacturer	Model	Range	Accuracy	Least count resolution
Differential pressure	Validyne	DP-15-26-N-1-5-4-A (signal conditioner: Validyne CD101-B-6-A-1-M)	0–3450 Pa (0–0.5 psi)	±0.25% full scale	0.81 Pa
Absolute pressure	Omega	PX303-050A 5V	0–345 000 Pa (0–50 psi)	±0.25% full scale	84.8 Pa
Temperature	Omega (signal conditioner: Analog Devices)	HYP4-16-1 1/2-100-E4-48-PR (signal conditioner: Analog Devices 5B350-02)	0–100°C	±0.1% full scale	0.1°C

of 30–60 min, and then measuring the captured volume with a syringe. Our instrument works on a similar principle but is more suitable for measuring flux over a large field of seepage because it is automated.

We describe the design, calibration, and deployment of an instrument for measuring gas flux to the ocean's surface from rising bubble plumes such as those that arise from marine hydrocarbon seeps. The instrument (hereinafter referred to as a flux buoy) measures flux using a gas-capture technique. Because our study area is the region of very strong seepage off of Coal Oil Point, the instrument is configured to measure high fluxes. The basic design, however, may be readily adapted for use in environments with much weaker gas flux.

A primary goal is to quantify the spatial distribution of methane seepage over continental shelves. Only the total volume flux of gas, not its composition, is measured by the flux buoy, so quantifying the flux of particular gases such as methane requires ancillary compositional analysis. Chanton et al. (1988) found that the volume fraction of methane bubbling from estuarine sediments varied within a range of 55%–80% depending on bubbling flux rate, the amount of vegetation, and season. Analysis of gases collected near the sea surface around the Coal Oil Point seeps showed methane volume fractions of about 60% (Leifer et al. 2000). The total gas flux measured by the flux buoy must be corrected by these fractions to derive methane flux. If the fraction of methane in the captured gas varies substantially, such as reported by Chanton et al. (1988), then extensive measurements of gas composition would be necessary to constrain methane flux rates. The few surface analyses of gas composition available from the Coal Oil Point seep field suggest the volume fraction of methane is fairly constant (Leifer et al. 2000).

The rest of the paper is organized as follows: section 2 describes the flux buoy design and operation; field deployments are also described in section 2; laboratory calibrations are discussed in section 3; results from field trials are explained in section 4. Section 5 summarizes the instrument characteristics and performance.

2. Buoy design, construction, and operation

The flux buoy measures gas flux by capturing gas bubbles a few meters below the sea surface. Bubbles from rising plumes are directed into a collection chamber through a circular cone at the base of the flux buoy (Fig. 1). As gas accumulates in the collection chamber, a gas–water interface forms, then descends at a rate proportional to the volume flux of gas. The pressure difference Δp between the inside of the collection chamber and surrounding seawater (hereinafter referred to as differential pressure) is

$$\Delta p = (\rho - \rho_g)gh \approx \rho gh, \tag{1}$$

where ρ is the seawater density, ρ_g is the density of the gas in the chamber ($\rho_g \ll \rho$), g is the acceleration of gravity, and h is the distance between the measured gas–water interface and the top of the collection chamber. The volume flux of gas per unit area of sea surface, adjusted to standard temperature T_a and pressure p_a, is

$$\dot{q} = (\rho g)^{-1} \frac{\partial \Delta p}{\partial t} \frac{T_a}{T_c} \frac{p_c}{p_a} \frac{A_c}{A_{\text{co}}}, \tag{2}$$

where $\partial \Delta p/\partial t$ is the time rate of change of differential pressure, T_c and p_c are temperature and pressure of the gas in the collection chamber, A_c is the area of the collection chamber, and A_{co} is the area of the collecting cone (0.27 m^2). Ideal gas behavior has been assumed.

Gas accumulates in the chamber until an adjustable threshold Δp is reached. Then a microcomputer-controlled valve opens to release the accumulated gas and start a new measurement cycle. Gas vents through a port at the base of the electronics pressure case that also contains the sensors, electronics, and microcomputer (Fig. 1). The buoyancy loss from the small volume of gas vented from the chamber does not significantly affect the buoy's vertical position in the water. The threshold Δp is set to prevent filling the chamber and spilling gas out of the open bottom. The valve can also be opened at any time remotely from the research boat.

Data acquisition, valve operation, and data transmission are controlled by a Blue Earth Research, LLC, Micro485 microcontroller. This small computer includes four 12-bit analog-to-digital (A/D) channels (0–5-V range), battery backed-up static random access memory (RAM), clock, digital input/output, RS422 (recommended standard No. 422) serial communications, and a BASIC interpreter. The control program can be uploaded to the computer via the serial communication

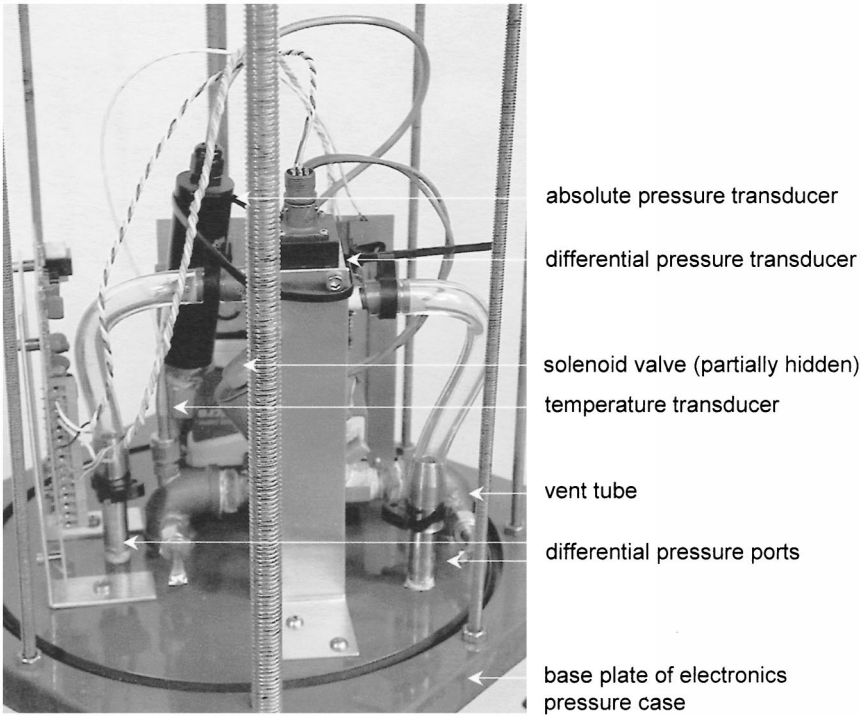

FIG. 2. Interior of electronics pressure case, identifying temperature and pressure transducers.

link and stored in RAM. The program runs automatically upon power-up, which is a useful characteristic because the electronics are sealed in the electronics pressure case. The computer samples Δp, T_c, and p_c once per second.

Gas vents through a tube (Fig. 2) opened by a 12-V solenoid valve (Automatic Switch Company, model 8030B-12V) with an opening large enough to empty the collection chamber in less than 1 s. The microcontroller opens the valve through a metal-oxide semiconductor field effect transistor (MOSFET) switch when the vent Δp threshold is exceeded.

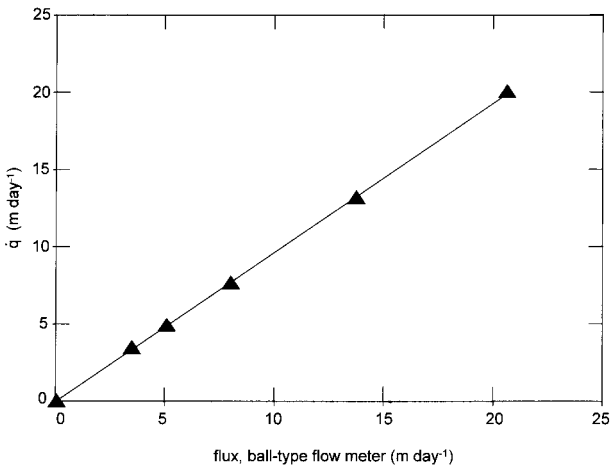

FIG. 3. Calibration of flux buoy from swimming pool tests: *x* axis shows flux measured with ball-type flow meter and *y* axis shows flux $\dot{q}$ derived from flux buoy using (2). Slope of fitted line is 0.96.

Finding a suitable differential pressure transducer proved difficult because of the requirements for corrosion resistance for use in seawater and high sensitivity for resolving small pressure differences. The first sensor we tried used two gauge-type transducers with differential electronics. Tests in a swimming pool revealed that this sensor had poor stability and was unsuitable. A second sensor using a variable reluctance scheme performed successfully. Table 1 summarizes the characteristics of this sensor and the other pressure and temperature transducers used on the flux buoy; Fig. 2 shows their arrangement in the electronics pressure case.

The electronics pressure case is a polyvinyl chloride (PVC) cylinder (pipe section), 0.25 m in diameter and 0.26 m long with a wall thickness of 7 mm. It is capped on both ends with PVC plates, 24 mm thick. The lower plate (base plate, shown in Fig. 2) is square, the upper plate is octagonal, and both are 0.31 m across. O-rings seal the plates on the ends of the cylinder. Sections of threaded rod, 7 mm in diameter, extend along the cylinder though the plates; nuts on the threaded rods compress the plates to seal the pressure case. A clear Plexiglas window on the upper plate permits inspection of the sensors and electronics without opening the pressure case. A bulkhead connector penetrates the upper plate and connects the data-transmission cable to the electronics. Ports in the base plate expose the temperature sensor, absolute pressure sensor, and one side of the

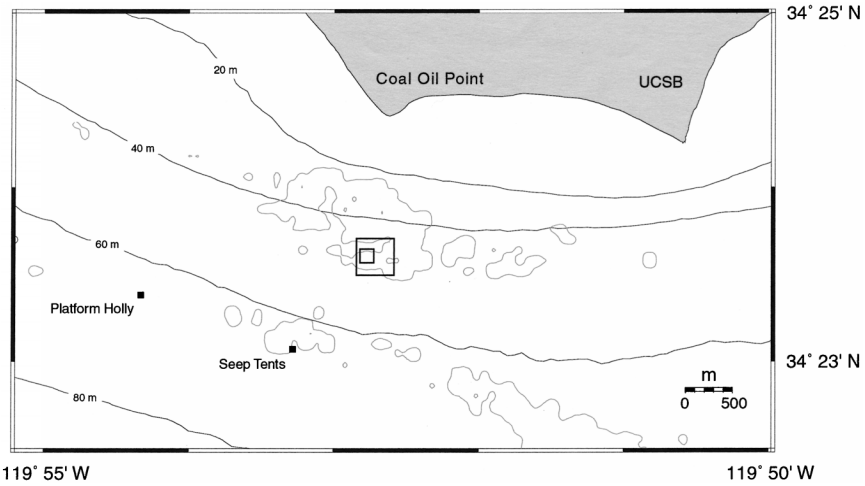

FIG. 4. Study area off Coal Oil Point near Santa Barbara, CA. Closed contours indicate areas of hydrocarbon seepage activity obtained from sonar surveys described by Quigley (1997) and Quigley et al. (1999). Bathymetric contours at 20, 40, 60, and 80 m are indicated. Larger square shows area of Fig. 8, smaller square shows area of Fig. 9. Platform Holly is an oil production platform. The seep tents are large pyramidal structures on the sea floor to capture natural gas.

differential pressure sensor to gas and seawater at the top of the collection chamber. Another port through the base plate exposes the other side of the differential pressure sensor to seawater pressure outside the collection chamber.

The collection chamber, made of clear polycarbonate plastic, is cemented to a PVC flange; the flange attaches with bolts threaded into the bottom of the base plate. An O-ring seals the flange to the base plate to prevent gas leakage. The chamber can be changed easily in the field to accomodate different flux rates. Two chambers have been used in our field experiment with areas $A_c = 1.6 \times 10^{-3}$ and 7.1×10^{-3} m^2; the larger chamber is used in areas with the highest volume flux. The cone for directing gas into the collection chamber is 0.58 m in diameter and made of high-density polyethylene plastic. It was cut from a liquid storage tank with a conical bottom. The cone diameter is much larger than seep bubble diameters in the plumes (typically ≤ 1 cm; Quigley 1997). A small metal cone is attached to the apex of the plastic cone with its outlet at the base of the collection chamber. Four sections of threaded rod, 0.97 m long and 12 mm in diameter, join the cone to the gas-capture assembly (pressure case, electronics, sensors, collection chamber). They extend from four brackets on the cone, through the base plate of the pressure case, to 0.11 m above the pressure case. Tensioned cables diagonally connect the threaded rods to stiffen the gas-capture assembly. The spar buoy attaches to the upper ends of these rods.

The spar buoy is constructed from PVC pipe, 0.09 m in diameter and 3.1 m long. The upper end of the pipe is sealed with a cap and the lower end with a PVC flange mounted on a fiberglass plate. Holes in the fiberglass plate engage the four sections of threaded rod extending above the pressure case. A collar of closed-cell foam mounted on the spar buoy provides additional flotation (Fig. 1). Four dive weights totaling 18 kg are attached to the cone at the base of the buoy for ballast.

The long, narrow configuration of the flux buoy dampens motions due to small-amplitude, high-frequency surface waves. Its natural period of oscillation is 14 s as determined in a series of ''bounce tests'' in a swimming pool. This is longer than the periods of waves encountered during field deployments (5–8 s) conducted in conditions of light wind and low swell. During field deployment about 1.3 m of the buoy extends above the sea surface. The top of the collection chamber is about 2.6 m below the sea surface.

Buoy position is logged every 2 s with a differential Global Positioning System (GPS) receiver (GPS receiver, GARMIN International Corporation model 45; differential beacon receiver, GARMIN model GBR21) mounted near the top of the buoy in a waterproof box (Fig. 1). Antennas for receiving the GPS and differential beacon signals attach to the top of the waterproof box. A plastic window in the cover of the waterproof box allows observation of the GPS receiver's display. Data from the gas collector and GPS receiver are separately transmitted by cables via RS422 to the research boat and converted to RS232 before logging and display on a computer. During postcruise processing, GPS position data are smoothed with a fifth-order, low-pass Butterworth filter with a cutoff (half power) frequency of 0.033 Hz (30-s period). Data from the gas collector and GPS receiver are merged in software based on time. In field operations the buoy either is allowed to drift freely or is gently towed on a bridle (Fig. 1) through seepage areas as the research boat moves slowly forward.

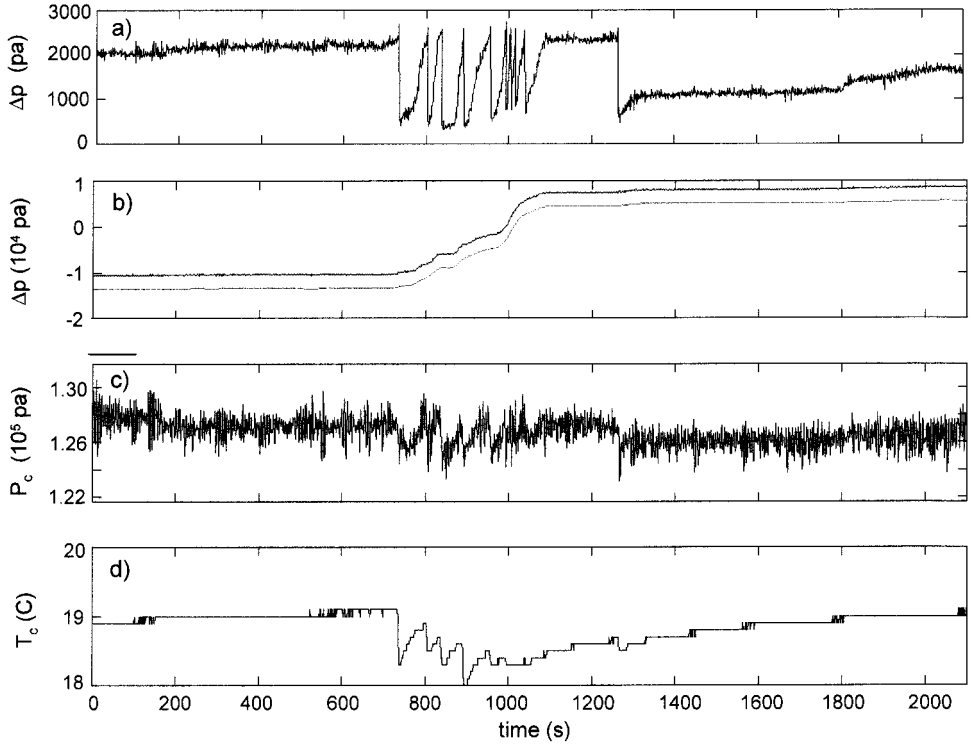

FIG. 5. Times series for drift 2 on 8 Jul 1999 of (a) Δp (discontinuities indicate venting of gas from collection chamber, (b) Δp [discontinuities are removed and mean is set to zero; lower curve shows same time series offset by 3000 Pa and smoothed with a 5-pole low-pass Butterworth filter with cutoff frequency 0.022 Hz (45-s period)], (c) p_c, and (d) T_c.

3. Buoy calibration

Pressure sensors were calibrated in the laboratory prior to the field deployments by connecting a manometer to the differential and absolute pressure ports. Hydrostatic pressure measured with the manometer was compared with digital counts from the A/D converters for Δp and p_a over the ranges 0–1900 and 102 000–132 000 Pa, respectively (Egland 2000). The responses of both sensors were linear over the range of pressures encountered during field sampling.

To verify operation of the buoy as a flux-measuring instrument, tests were conducted in a swimming pool using a metered bubbling gas (nitrogen) source with adjustable volume-flow rate. During the tests, the buoy floated freely in the pool on a slack tether. Nitrogen was fed through a ball-type flow meter and tubing to a porous air stone placed on the pool bottom, below the buoy. Manual adjustment of a valve in the line to the flow meter produced a range of flow rates. After each adjustment the system was allowed to run for a few minutes before recording the rate from the ball flow meter. Egland (2000) discusses the pool-calibration procedure in more detail.

In the flux range 0–20 m day^{-1} (0–$\sim$2 $\times$ 10^{-4} m s^{-1}), $\dot{q}$ estimated from (2) nearly equaled $\dot{q}$ computed from the ball flow meter (Fig. 3); the slope of the best-fit line relating the two is 0.96. At greater flow rates the buoy underestimated $\dot{q}$ because the collection chamber filled so rapidly that gas escaped out the chamber bottom before complete venting occurred. Fluxes above 20 m day^{-1} were not encountered in our field experiments, but use of a larger collection chamber could prevent overflow in regions of very high flux.

4. Field experiments

Several field trials of the buoy were conducted in the region of strong hydrocarbon seepage off Coal Oil Point during the autumn of 1998 and summer of 1999 (Fig. 4). Each field experiment consisted of a series of drifts of the buoy along tracks up to several hundred meters long. Most drift tracks crossed regions of strong hydrocarbon seepage visually identifiable by bubble plumes at the sea surface. A few tracks were obtained away from areas of seepage to evaluate the effects of surface waves and buoy motion. We present representative results from field experiments on 8 July and 19 August 1999.

Examples of time series of Δp, p_c, and T_c obtained from the flux buoy on 8 July 1999 are shown in Fig. 5 from a region of strong bubbling gas flux emanating from the Coal Oil Point anticlines (Fischer 1977; Hor-

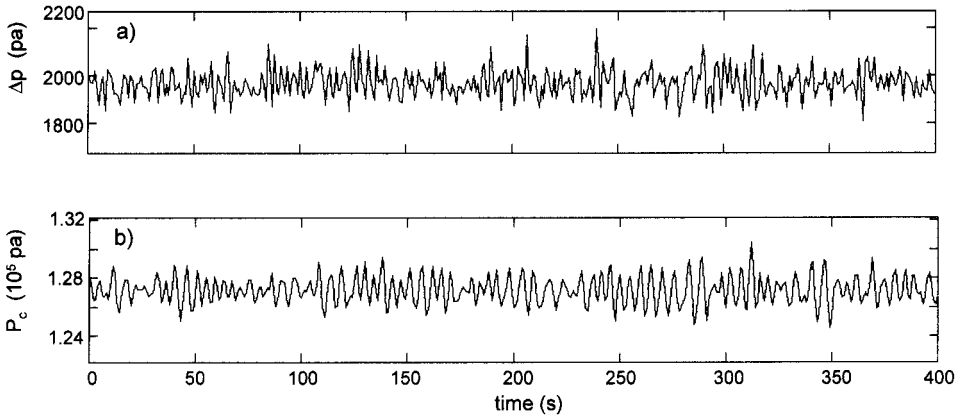

FIG. 6. A portion of times series for drift 2 on 19 Aug 1999 of (a) Δp and (b) p_c that shows the effects of surface waves. No venting of gas from the collection chamber occurred during this record, and no seepage was encountered.

nafius et al. 1999; Quigley et al. 1999). Steep increases in Δp occurred when the buoy was over the strongest bubble plumes and the collection chamber filled rapidly (Fig. 4a). Abrupt drops lasting less than 1 s in the Δp time series (i.e., less than the sampling interval) correspond to venting of the collection chamber. To permit digital filtering and other analysis, these pressure drops were removed in data processing to produce an approximately monotonic time series (Fig. 5b, upper curve). In the removal procedure, the value of Δp just before a drop was added to those after the drop; subsequent drops were similarly removed.

Temperature in the collection chamber also dropped abruptly during venting: at the first valve opening in Fig. 5d, T_c dropped 0.8°C from an initial value of 18.9°C. The source of the colder water was upwelling within the bubble plumes where ''boils'' and strong surface divergences were observed. Laboratory studies have shown that turbulent bubble plumes in stratified environments can entrain, mix, and upwell ambient wa-

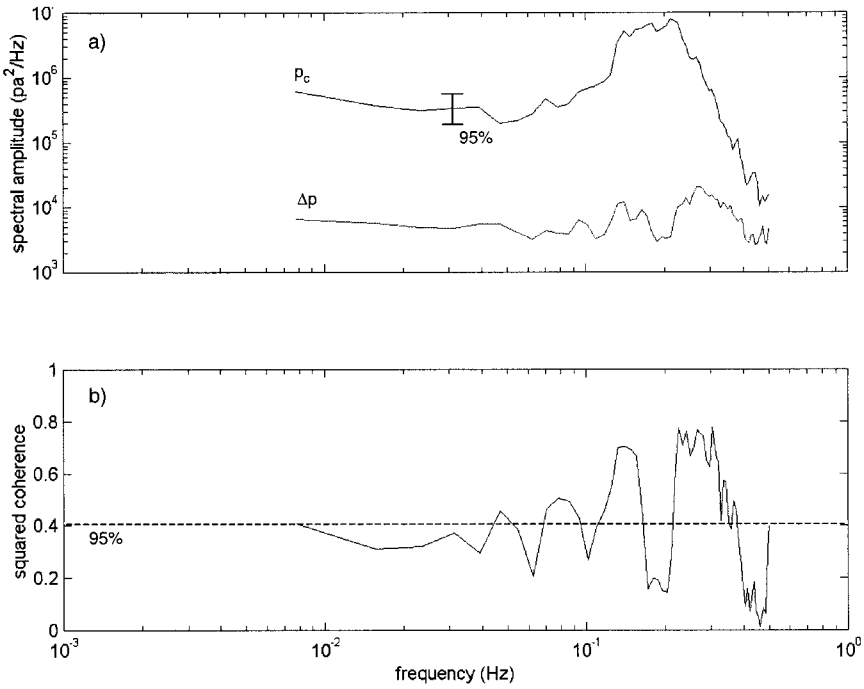

FIG. 7. (a) Autospectra of p_c (upper curve) and Δp for time series of Figs. 5b and 5a, respectively. Bar shows 95% confidence interval for spectral amplitudes. (b) Squared coherence between absolute and differential pressure time series. Coherence above dashed line is significant at 95% level.

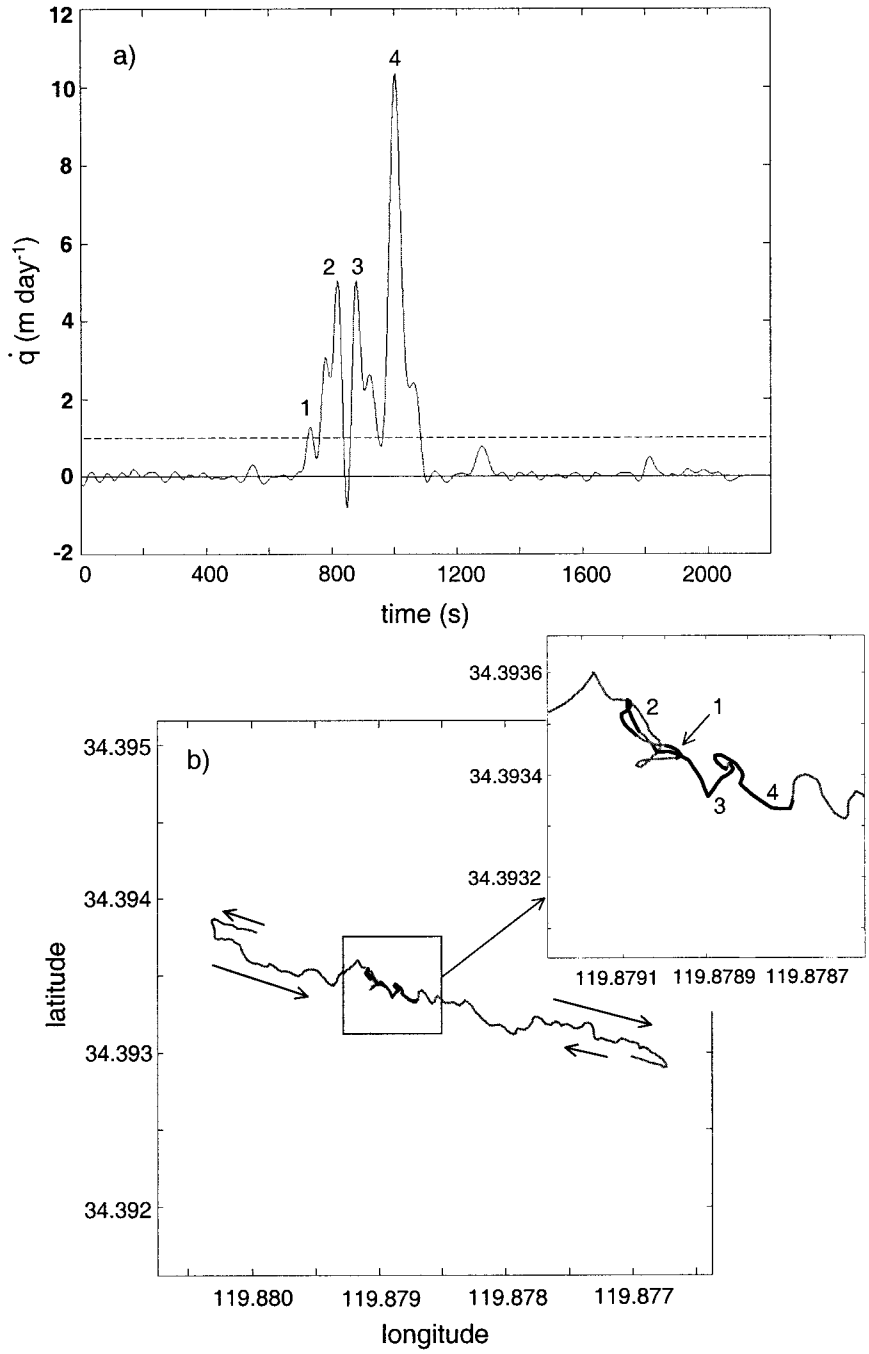

FIG. 8. (a) The $\dot{q}$ for drift 3 on 8 Jul 1999. (b) Drift track of flux buoy. Dark line indicates $\dot{q} > 1$ m day^{-1} (dashed line). Square is 400 m on a side. Inset shows close-up view of buoy track. Smaller square is 70 m on a side.

ters from depth (Asaeda and Imberger 1993; McDougall 1978). After each venting, T_c increased as gas accumulated in the chamber. The gradual increase in temperature evident in Fig. 5d after the bubble plumes were crossed likely resulted from drift of the buoy out of the cool, upwelled plume. Steps in temperature are artifacts from the A/D conversion.

Ideally, surface waves and buoy motion would have no effect on Δp since they produce equal pressure fluctuations inside and outside the chamber. High-frequency fluctuations are evident in the Δp time series, however, consistent with small surface waves (Fig. 5a). Fluctuations with periods of 4–6 s are prominent in the time series of p_c with standard deviation $\sigma_{p_c} = 867$ Pa (~5

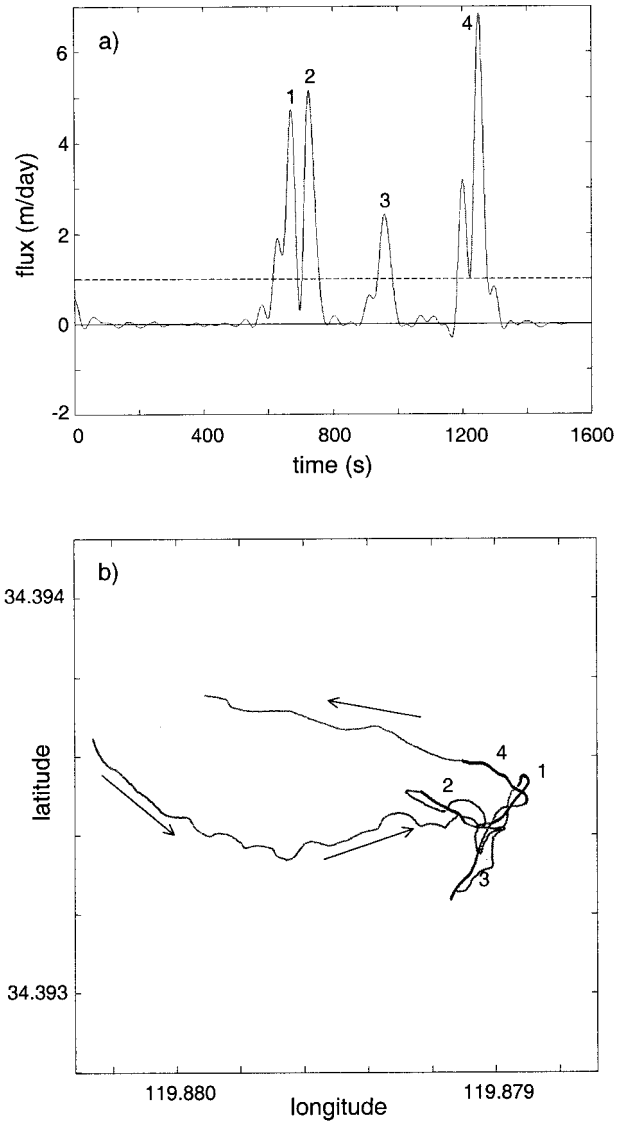

FIG. 9. As in Fig. 8, but for drift 2 of the flux buoy on 8 Jul 1999. The square in (b) is 150 m on a side.

cm wave amplitude) over the first 500 s (Fig. 5c). Because gas flux estimates are proportional to $\partial\Delta p/\partial t$ by (2), they are sensitive to these pressure fluctuations. To investigate the effects of waves and buoy motion, time series of Δp and p_c were obtained on 19 August 1999 in a region without measurable seepage activity (Figs. 6a,b). Temperature was nearly constant over the record (data not shown). Chamber pressure p_c fluctuated about a mean of 127 170 Pa with $\sigma_{p_c} = 1080$ Pa (Fig. 6b); fluctuations in Δp were much lower (Fig. 6a) with $\sigma_{\Delta p} = 63$ Pa. The spectrum of p_c for the record has a broad peak in the frequency range 0.12–0.28 Hz (periods of ~4–8 s) consistent with surface waves (Fig. 7a, upper curve). At lower frequencies, the spectrum is approximately white. The Δp spectrum is also nearly white, with low, broad spectral peaks centered at 0.15 and 0.27 Hz (Fig. 7a, lower curve). Spectral amplitudes of Δp are generally lower than those of p_c by factors of 100 or more.

Squared coherence between Δp and p_c indicates that fluctuations in these quantities are significantly correlated in the surface-wave frequency range of 0.21–0.38 Hz and near 0.14 Hz (Fig. 7b). Thus, we conclude that surface waves and buoy motion are a significant source of noise in our measurements of Δp. Noise in the time series of Δp was reduced by applying a fifth-order, low-pass Butterworth digital filter. After experimenting with a range of cutoff frequencies f_c, we determined that f_c in the range of 0.02–0.05 Hz was a good compromise between smoothing and along-track resolution. Results presented here use $f_c = 0.022$ Hz (45-s period). The lower curve of Fig. 5a shows an example of a smoothed Δp time series. Volume flux, $\dot{q}$ is computed from (2), where the partial derivative $\partial\Delta p/\partial t$ is estimated from a first difference of the smoothed Δp time series.

Time series of $\dot{q}$ for the data record of Fig. 5 clearly show areas of strong seepage flux, with a maximum of about 10 m day^{-1} (Fig. 5a, lower curve; Fig. 8a). The buoy track corresponding to this time series was 530 m long (Fig. 8b). The buoy was towed in tightly curving arcs through the areas of strongest seepage to maximize data collection there. The mean flux along the track is $\bar{\dot{q}} = 0.56$ m day^{-1}. For comparison, Quigley (1997) estimated a mean flux in the range (3.7–6.2) $\times 10^{-2}$ m day^{-1} over the entire seep-field area (~3 km^2). A second flux time series (Fig. 9), also from 8 July 1999 and in the same seepage area (Fig. 1), shows three intervals of high flux, with a maximum of almost 7 m day^{-1}. Peaks labeled 1 and 4 were encountered in about the same place where the buoy track doubled back on itself (Fig. 9b). The track length is 381 m and the along-track mean flux is $\bar{\dot{q}} = 0.58$ m day^{-1}, similar to other estimates.

Flux noise levels $\dot{q}_n$, due to buoy motion and surface waves are typically much smaller than $\dot{q}$ in the bubble plumes. We estimate $\dot{q}_n$ from a 1200-s record, part of which is shown in Fig. 6, where all fluctuations result from buoy motion and surface waves. This record is typical of those obtained under conditions of light winds and small waves off Coal Oil Point. For the record of Fig. 6, $\dot{q}_n = (0.3 \pm 6) \times 10^{-2}$ m day^{-1}. Over the first 500 s of the record of Fig. 5, before the bubble plumes were crossed, $\dot{q}_n = (0.1 \pm 8) \times 10^{-2}$ m day^{-1}. Occasional large negative values of $\dot{q}_n$ result from accidental tugs on the towing bridle as the research boat maneuvered the buoy through the bubble plumes (e.g., 850 s in Fig. 8a). Fluctuations in $\dot{q}_n$ with periods in the range of 50–70 s are evident in Fig. 8a before and after the bubble plumes were crossed. These probably resulted from low-frequency vertical motions of the buoy.

5. Summary

We have developed a buoy and gas-capture assembly, referred to as a flux buoy, for direct measurement of

gas flux from rising bubble plumes in oceans and lakes. We are using the flux buoy to quantify gas flux to the atmosphere in regions of strong hydrocarbon seepage over the continental shelf. An extensive series of flux measurements have been obtained in the region of hydrocarbon seepage off Coal Oil Point near Santa Barbara, California. The maximum flux observed for seeps in the Coal Oil Point anticline is on the order of 10 m day^{-1}. During calibration tests in a swimming pool, the buoy was capable of measuring fluxes up to 20 m day^{-1}; use of larger collection chambers would permit measurement of higher fluxes. The lowest detectable fluxes depend on sea state and the resulting vertical motion of the buoy. For conditions of light wind and small swell off Coal Oil Point, typical mean noise levels are in the range $(0.1–0.3) \times 10^{-2}$ m day^{-1} with standard deviation $(6–8) \times 10^{-2}$ m day^{-1}.

The gas-capture assembly can be operated independently of the buoy for applications such as deployment over gas vents on the seafloor or lakebeds. A smaller version of the buoy could also be made for deployments in small bodies of water on which surface wave effects are minimal.

Acknowledgments. We thank David Farrar and Shane Anderson for skillful operation of the research boat during field experiments. David Salazar assisted with preparations and field deployments. Ira Leifer and Jordan Clark provided useful comments on a draft of the manuscript. We had helpful discussions with Bruce Luyendyk and Jim Boles during the development of the buoy. This research was funded by the University of California Energy Institute.

REFERENCES

Asaeda, T., and J. Imberger, 1993: Structure of bubble plumes in linerly stratified environments. *J. Fluid Mech.,* **249,** 35–57.

Chanton, J. P., C. S. Martens, and C. A. Kelley, 1988: Gas transport from methane-saturated, tidal freshwater and wetland sediments. *Limnol. Oceanogr.*, **34,** 807–819.

Crill, P. M., K. B. Bartlett, J. O. Wilson, D. I. Sebacher, J. M. Melack, S. MacIntyre, L. Lesack, and L. Smith-Morrill, 1988: Tropospheric methane from an Amazonian floodplain lake. *J. Geophys. Res.,* **93** (D2), 1564–1570.

Egland, E. T., 2000: Direct capture of gaseous emissions from natural marine hydrocarbon seeps offshore of Coal Oil Point, Santa Barbara, California. M.S. thesis, Dept. of Geological Sciences, University of California, Santa Barbara, 67 pp.

Fischer, P. J., 1977: Natural gas and oil seeps, Santa Barbara basin, California. California offshore gas, oil, and tar seeps, State of California, State Lands Commission, Sacramento, Staff Report, 449 pp.

Freeth, S., and R. L. F. Kay, 1987: The Lake Nyos gas disaster. *Nature,* **325,** 104–105.

Hornafius, J. S., D. C. Quigley, and B. P. Luyendyk, 1999: The world's most spectacular marine hydrocarbon seeps (Coal Oil Point, Santa Barbara, California): Quantification of emissions. *J. Geophys. Res.,* **104** (C9), 20 703–20 711.

Hovland, M., A. G. Judd, and J. Burke, 1993: The global flux of methane from shallow submarine sediments. *Chemosphere,* **26** (1–4), 559–578.

Kanari, S.-I., 1989: An inference on the process of gas outburst from Lake Nyos, Cameroon. *J. Volcanol. Geotherm. Res.,* **39,** 135–149.

Leifer, I., J. F. Clark, and R. F. Chen, 2000: Modification of the local environment by natural marine hydrocarbon seeps. *Geophys. Res. Lett.,* **27,** 3711–3714.

MacDonald, I. R., 1998: Natural oil spills. *Sci. Amer.,* **279,** 56–61.

McDougall, T. J., 1978: Bubble plumes in stratified environments. *J. Fluid Mech.,* **85,** 655–672.

Oremland, R. S., L. G. Miller, and M. J. Whiticar, 1987: Sources and flux of natural gases from Mono Lake, California. *Geochem. Cosmochim. Acta,* **37,** 2915–2929.

Quigley, D. C., 1997: Quantifying spatial and temporal variations in the distribution of natural marine hydrocarbon seeps in the Santa Barbara Channel, California. M.S. thesis, Dept. of Geological Sciences, University of California, Santa Barbara, 95 pp.

——, J. S. Hornafius, B. P. Luyendyk, J. F. Clark, and L. Washburn, 1999: Decrease in natural marine hydrocarbon seepage near Coal Oil Point, California, associated with offshore oil production. *Geology,* **27,** 1047–1050.

Romero, J., J. C. Patterson, and J. M. Malack, 1996: Simulation of the effect of methane bubble plumes on vertical mixing in Mono Lake. *Aquat. Sci.,* **53** (3), 210–223.

Sebacher, D. I., and R. C. Harriss, 1982: A system for measuring methane fluxes from inland and coastal wetland environments. *J. Environ. Qual.,* **11,** 34–37.

Simoneit, B. R. T., P. F. Lonsdale, J. M. Edmond, and W. C. Shanks III, 1990: Deep-water hydrocarbon seeps in Guaymas Basin, Gulf of California. *Appl. Geochem.,* **5,** 41–49.

Woods, A. W., and J. C. Phillips, 1999: Turbulent bubble plumes and CO_2-driven lake eruptions. *J. Volcanol. Geotherm. Res.,* **92,** 259–270.